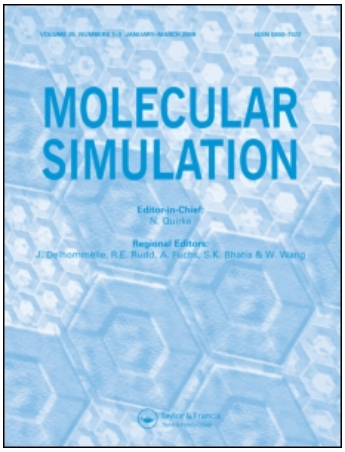

Molecular Simulation
Publication details, including instructions for authors and subscription information:
http://www.informaworld.com/smpp/title~content=t713644482

Proton transport in water confined in carbon nanotubes: a reactive molecular dynamics study

M. Esai Selvan[a]; D. J. Keffer[a]; S. Cui[a]; S. J. Paddison[a]
[a] Department of Chemical and Biomolecular Engineering, University of Tennessee, Knoxville, TN, USA

Online publication date: 03 August 2010

To cite this Article Esai Selvan, M. , Keffer, D. J. , Cui, S. and Paddison, S. J.(2010) 'Proton transport in water confined in carbon nanotubes: a reactive molecular dynamics study', Molecular Simulation, 36: 7, 568 — 578
To link to this Article: DOI: 10.1080/08927021003752887
URL: http://dx.doi.org/10.1080/08927021003752887

Molecular Simulation
Vol. 36, Nos. 7–8, June–July 2010, 568–578

Taylor & Francis
Taylor & Francis Group

Proton transport in water confined in carbon nanotubes: a reactive molecular dynamics study

M. Esai Selvan, D.J. Keffer*, S. Cui and S.J. Paddison

Department of Chemical and Biomolecular Engineering, University of Tennessee, Knoxville, TN 37996-2200, USA

(*Received 15 December 2009; final version received 5 March 2010*)

The effects on the structural and transport properties of a proton in water confined in carbon nanotubes of radii ranging from 5.42 to 10.85 Å were studied by employing a recently devised reactive molecular dynamics (RMD) scheme. The formation of distinct layers was observed in the computed radial density profile of water. Affinity of hydronium ions towards the tube–water interface and its preferential orientation with the oxygen atom protruding towards the wall was observed. The axial water diffusivity was observed to decrease with increasing confinement of water. Analysis of the axial charge diffusivity and its two components (structural and vehicular) was also performed. Confinement was found to have a more significant effect on structural diffusion than on vehicular diffusion. The axial vehicular component of the charge diffusivity in the nanotube of radius 10.85 Å was found to be equal to the value computed in bulk water while structural component was 12% of the value observed in bulk water, which resulted in a total charge diffusivity of 42% of the diffusion in bulk water. The confined geometry affects the system energetically and perturbs the solvation structure around the proton from that found in bulk water. The RMD algorithm, which defines the occurrence of a proton transfer reaction based on the satisfaction of a set of triggers, identified the energetic factor to be greatly responsible for the decreased structural diffusion of a proton.

Keywords: proton transport; structural diffusion; carbon nanotubes; confinement

1. Introduction

Proton transport is a key process in many chemical (acid–base solutions), biological (proteins and enzymes) and electrochemical [proton exchange membranes (PEM)] systems and hence a fundamental understanding of this process will benefit a wide range of applications. One of the potential applications of proton transport includes the energy conversion in PEM fuel cells. Many PEM fuel cells use perfluorinated sulphonic acid polymers (e.g. Nafion, Flemion and Aciplex) as electrolytes, which have a perfluorinated backbone and pendant side chains containing sulphonic acid (SO_3H) groups. Hydration of the materials leads to a spontaneous segregation into hydrophobic (perfluorinated backbone) and hydrophilic regions (water and charged side groups) whose characteristic dimensions are of the order of nanometres. It is through the hydrophilic domain networks that the proton is transported. Therefore, understanding the relationship between proton transport and the hydrated morphology, which is governed by the polymer structure [1,2], is important in the development of economically viable PEM fuel cells.

There is a significant understanding of the molecular-level mechanisms of proton transport in bulk water. The proton is transported via both structural diffusion [3,4] and mass diffusion as hydronium ions (vehicular diffusion). Structural diffusion involves the hopping of protons from one water molecule to another via structural defects [5]. The hopping mechanism is responsible for the high mobility of protons compared to other cations of similar size and charge in aqueous media [6]. Structural diffusion of the proton in aqueous media occurs by the continual interconversion of two predominant structures of Zundel [7] ($H_5O_2^+$) and Eigen [8] ($H_9O_4^+$) cations with the cleavage and formation of the hydrogen bonds in the second solvation shell [3,9].

The aqueous domains within PEMs differ from bulk water in two important ways. First, the proton is in a highly acidic environment and, second, the proton is in a confined fluid. The effects of confining the proton transport to very small aqueous regions are not completely understood. However, both experimental and modelling studies have revealed that the water in PEMs exhibits a decreased polarity and rate of relaxation and an increase in the degree of the spatial and orientational order when compared to bulk water [10–13]. We have examined systems in which the acidity and confinement can be independently varied to better understand how these two factors, acidity and confinement, impact proton mobility. Previously, we investigated the effects of acidity on proton transport in aqueous solutions of HCl [14]. In the present study, we examine only the effect of confinement on proton transport in dilute acidic solutions in carbon nanotubes (CNTs). This ability to distinguish between the impact of acidity and confinement on proton transport may help to understand the cumulative behaviour of proton transport in PEMs, where both acidity and confinement are present.

*Corresponding author. Email: dkeffer@utk.edu

ISSN 0892-7022 print/ISSN 1029-0435 online

DOI: 10.1080/08927021003752887
http://www.informaworld.com

Currently, there is evidence from theory and simulation that both proton transport mechanisms are active in PEMs [15–19]. However, the extent to which these two mechanisms function in an environment with high local density of acidic groups is unclear [20,21]. Recent investigations employing *ab initio* molecular dynamics (AIMD) simulations of proton transport in the mono-, di- and tetra-hydrates of trifluoromethanesulphonic acid substantiate the evidence that structural diffusion occurs in systems with very high densities of SO_3H and encapsulated water [22,23].

Various modelling techniques such as Car–Parrinello AIMD [4,24], mixed quantum and classical mechanics techniques [25,26] (QM/MM), various empirical valence bond (EVB) schemes [27–30], a mixed MD/MC algorithm [31] and the Q-HOP MD method [32] have been devised to investigate proton transport. We have chosen to utilise a reactive molecular dynamics (RMD) algorithm, which has been applied previously to study proton transport in bulk water [14] as well as the thermal decomposition of perfluorodimethyl ether [33]. Using the RMD algorithm, the effect of acidic environment on the mechanisms of proton transport has already been investigated by the implementation of the algorithm in aqueous HCl systems of concentrations ranging from 0.22 to 0.83 M [14]. One advantage of the RMD algorithm is that, although it was parameterised in bulk water, it can be applied to bulk HCl solutions or to transport in CNTs without reparameterisation, because, at least to the coarse-grained level of description contained within the algorithm, it is able to directly account for the impact of the local environment on the reaction rate.

The transport properties of protons through water confined in CNTs of various diameters have been investigated earlier by AIMD simulations [34], classical MD simulations using potentials derived from *ab initio* calculations [35] and EVB models [36,37]. When the channels are very narrow (i.e. a (6,6) CNT of radius 4.07 Å), water wires are formed [34,37]. Proton diffusion through these well-aligned (defect-free) quasi-1D hydrogen-bonded water chains exceeds that in bulk water by a factor of 40 [37]. The influence of the electrostatic forces due to charge or polarity of the CNT leads to the formation of hydrogen-bonding defects in the water wire such as the L- and D-defects, which can drastically hinder the proton transfer mechanism [37]. A proton encapsulated within a water wire in a CNT is found to be highly stabilised but in the presence of an electric field, rapid diffusion is observed [34]. Once the CNT radius is large enough to have a 3D hydrogen-bonded water network, the proton diffusivity is sensitive to the channel radius and increases with the decrease in confinement [36].

In this work, the RMD algorithm has been applied to simulate proton transport through water confined in CNTs of radii from 5.42 to 10.85 Å to study the effect of confinement on the individual contribution of the component of the charge diffusion and to understand the probable reasons that can affect the structural diffusion of proton under confinement. CNTs play a pivotal role in a wide range of applications from membrane separations to drug delivery and hence understanding the effect of the confined CNT geometries on fluid transport properties has independent merit [38].

The paper is organised as follows: the methodology, including a brief description of the RMD algorithm and the details of the simulations are described in Section 2, the results and discussion are presented in Section 3 and the conclusions are summarised in Section 4.

2. Method

The structural diffusion of a proton is modelled with the RMD algorithm, whose details are presented in our earlier work [14,33]. A short description of the method is given here. The proton transfer process can be written as the following chemical reaction:

$$H_3O^+ + H_2O \overset{n_{H_2O}}{\longleftrightarrow} H_2O + H_3O^+. \quad (1)$$

Chemical reactions occur when the reactant molecules are suitably oriented and have sufficient energy to overcome the activation barrier for the formation of the products. The RMD algorithm coarse grains the chemical reaction via three steps: (i) satisfaction of a set of geometric and energetic triggers, (ii) instantaneous reaction and (iii) local equilibration. We perform a classical MD time step in the RMD algorithm. At the end of each MD time step, the three steps of the RMD algorithm are implemented. The first step checks whether the reactants (H_2O and H_3O^+) satisfy a set of six geometric triggers and one energetic trigger. The functional form of these triggers indicates that the reactant is following a trajectory leading to the transition state, as determined by quantum mechanical calculations. In other words, satisfying a set of triggers ensures that one has the correct starting configuration for the reaction in Equation (1) to take place. For this specific reaction, the six geometric triggers dictate (1) a maximum separation between the O of the H_3O^+ ion and the O of the H_2O molecule participating in the reaction, $r_{OO,Zundel,max}$, (2) a minimum separation between the proton to be transferred and the O of the H_3O^+ ion, $r_{OH,Equilib}$, (3) collinearity of the O of the H_3O^+ ion, the O of the H_2O molecule and the proton to be transferred, θ_{OHO}, (4) proper H—O—H bond angles between the proton and H on the water molecules, in accord with sp^3 bond hybridisation, θ_{HOH}, (5) hydrogen bonding of the two non-transferring H on the H_3O^+ ion with O of solvating water molecules, $r_{OO,Eigen,max}$ and (6) hydrogen bonding of the two H atoms on the H_2O molecule with O of other

water molecules, $r_{OO,Hydration,max}$. The energetic trigger, $E_{a,f}$, ensures that the total energy of the proton to be transferred that is composed of the kinetic energy projected along the reaction axis and all components of the potential energy (intramolecular interactions and intermolecular – both Lennard-Jones (LJ) and electrostatic interactions) is sufficient to overcome the activation barrier for reaction. The numerical values of these triggers are tuned to the experimental reaction rate as a function of temperature to yield the correct activation energy and rate constant for bulk water. The schematic representation of the six geometric triggers is shown in Figure 1 and the trigger values are given in parenthesis. The first step of a reaction in the RMD algorithm is therefore the satisfaction of a set of triggers for a favourable starting configuration for the reaction to take place.

The RMD algorithm includes fewer details than the quantum mechanical studies and many more details than the macroscopic modelling. The RMD triggers represent a necessary and sufficient condition for reaction to take place and predict well the charge diffusivity in bulk water, but they may not be the only set of triggers capable of doing so. It is possible that an alternative set of triggers including, for example, coordination number of water molecules in the first solvation shell might also suffice, but that alternative has not been explored here. There are certainly more detailed characteristics of the proton hopping process that do not appear in the more coarse-grained RMD description. For example, recent studies indicate that the cleavage of an acceptor-type hydrogen bond of a water molecule in the first solvation shell (forming the Zundel complex) is the rate limiting step associated with partner exchange and the cleavage of a donor-type hydrogen bonds of the other two water molecules (in the first solvation shell) not involved in the reaction is likely to be associated with the actual proton transfer event [9]. The purpose of the RMD algorithm, like any coarse-grained procedure, is to capture the basic behaviour of the system with as few degrees of freedom as possible. Admittedly, in this procedure, the full

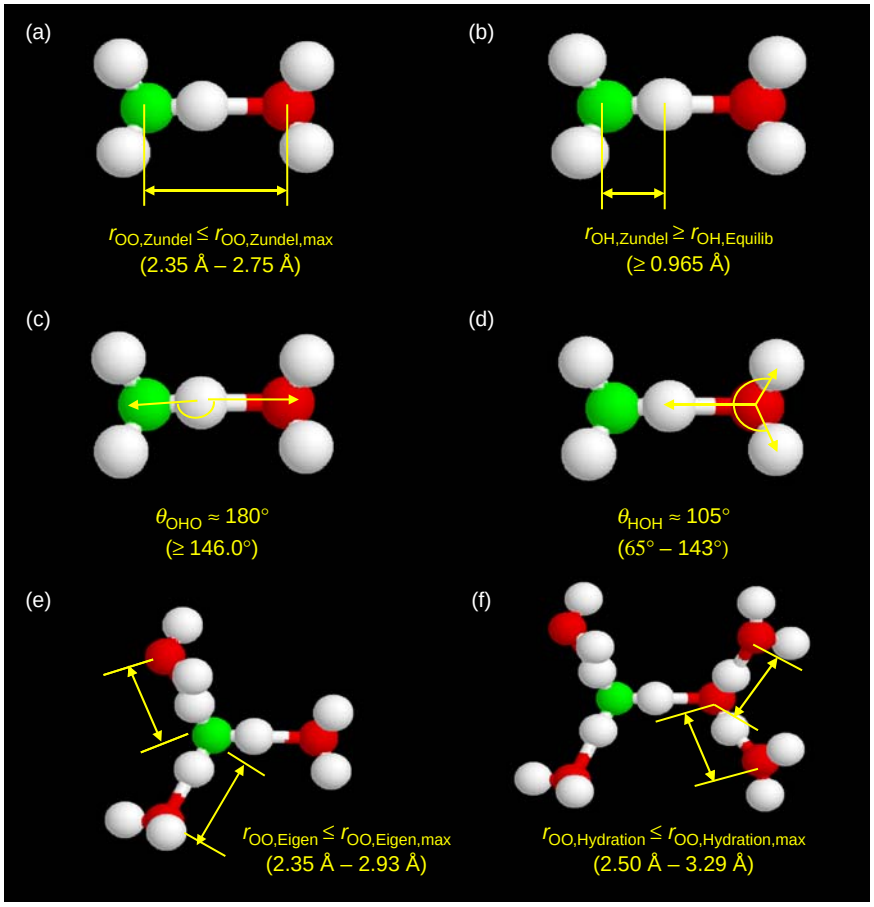

Figure 1. Graphical representation of six geometric triggers for structural diffusion: (a) O—O separation must form a Zundel ion, (b) O*—H separation must exceed the equilibrium bond distance, (c) ∠OHO is nearly linear in the Zundel ion, (d) lone pair of electrons in the water should point towards the proton, (e) initial H_3O^+ forms an Eigen ion and (f) Eigen ion is formed around final H_3O^+. These six geometric triggers must be satisfied along with the energetic trigger for the reaction to take place. The allowable range of the triggers is listed in parentheses. O of H_3O^+, green; O of H_2O, red; H, white.

quantum mechanical description of proton transport is not retained.

The second step of the RMD algorithm is the instantaneous reaction. Once the complete set of triggers has been satisfied by a given reactant, the RMD algorithm coarse grains the reaction path and the proton gets transferred instantaneously. The reaction involves exchanging the identities of the reactants, where the H_3O^+ that previously contained the proton to be transferred is now H_2O and the H_2O that received the proton is now a H_3O^+. The reaction takes places with no time elapsed in the MD simulation.

The third and final step of the RMD algorithm is the local equilibration. When a reaction takes place, structure and energy of the system are disturbed. The heat of reaction is zero for structural diffusion of proton. Therefore, the objective of the local equilibration is to ensure that one has the correct ending configuration of the product in Equation (1) and satisfy the target heat of reaction. The re-establishment of reasonable hydrogen-bonding network and energy of the system is achieved by relaxing the hydrating water molecules of the reactants with an objective function that has a weighted combination of both energetic and structural terms. Once structural diffusion is implemented by the RMD algorithm, the MD simulation continues onto the next time step.

The algorithm includes several proven beneficial effects as follows: (1) usage of computationally efficient classical MD simulation, (2) reduction in the development time required to parameterise the reactive algorithm, relative to reactive potentials, due to the decrease in the degrees of freedom and (3) extension of the methodology from one environment (bulk water) to another environment (aqueous HCl system or fluids confined in CNTs).

The accurate determination of the density of fluids under confinement is difficult since the inaccessible volume due to tube–wall interaction and void fraction due to the organised structure varies based on the choice of radius. There are various methods of determining the density of water [39]. One way is to immerse a nanotube segment into a large water bath where the water molecules are free to enter and exit the nanotube, so that one can obtain the natural density [40]. Another way is to perform simulations with fixed number of water molecules inside the nanotube based on the density of water (typically 1 g/cm^3) [36,41,42]. Here, we follow the latter and simpler method where the number of molecules needed in the system is fixed and the length of the CNT is determined from the bulk water density and accessible volume. The effective accessible radius is defined as the radius beyond which no water molecules exist due to the wall repulsion. The nanotubes are represented by a smooth external potential instead of modelling the walls atomistically with site-to-site interaction. Fluid–tube interactions have been modelled with a LJ potential integrated over the semi-infinite volume of the wall in cylindrical coordinates, as derived by Peterson et al. [43]. The fluid particle at a radial position, r, from the tube axis interacts with the tube wall of radius, R, using the potential, V_{ft},

$$V_{ft}(r,R) = \pi\varepsilon_{ft}\rho_t\left[\frac{7\sigma_{ft}^{12}}{32}K_9(r,R) - \sigma_{ft}^{6}K_3(r,R)\right], \quad (2)$$

where $K_m(r,R)$ is defined as

$$K_m(r,R) = R^{-m}\int_0^{\pi} d\Theta\left[-\eta\cos\Theta + (1-\eta^2\sin^2\Theta)^{1/2}\right]^{-m}, \quad (3)$$

and $\eta = r/R$. The Lorentz–Berthelot rule is applied to obtain the values of LJ mixture well-depth and collision diameter, ε_{ft} and σ_{ft}, from the pure component parameters. The number density of interaction sites in the carbon wall, ρ_t, is equal to 0.114 Å^{-3} [44]. The size and energy parameters of carbon (graphite) are 3.4 Å and 28 K, respectively [45].

Constant number of molecules, volume and temperature (NVT) simulations were performed for nanotubes of radii ranging from 5.42 to 10.85 Å at 300 K with an experimental bulk water density [46] of 0.9965 g/cm^3 within the accessible volume. We choose this temperature and this range of radii as they are relevant to the aqueous nanochannels present in PEMs [47]. The system contains 499 molecules of water along with one hydronium ion for an infinite dilution. For better statistics, 144 independent simulations were run at each state point with different initial configurations. Table 1 summarises the system sizes for each of the nanotubes studied. The radii studied correspond to armchair (R,R) CNTs with indices $R = 8$, 10, 12, 14 and 16. The TIP3P model [48] with flexible OH bond [49] is used for water, while the hydronium ion is represented using the same model with modified charges on the O and H atoms [50]. Electrostatic interactions were calculated using the reaction field method [51]. The cut-off distance for non-bonded interactions is 10 Å. The equations of motion are integrated using a two time-scale r-RESPA [52] with a large time step of 2 fs and a small time step of 0.2 fs. Periodic boundary conditions are enforced only in

Table 1. Physical dimensions of the simulated CNTs[a].

Tube radius (Å)	Length of tube (Å)	Radius accessible (Å)
5.42	364.29	3.62
6.78	200.46	4.88
8.14	124.59	6.19
9.49	82.87	7.59
10.85	60.81	8.86

[a] All simulations have been performed at 300 K and a density of 0.9965 g/cm^3 with 500 molecules of H_2O or 499 H_2O molecules and 1 H_3O^+ cation.

the axial direction of the tube (z-axis) to yield an infinite long channel. Constant temperature was maintained by incorporating a Nosé–Hoover thermostat [53–55] with a frequency of $0.01\,\mathrm{fs}^{-1}$. The high frequency aids the removal of excess heat that was not removed by the local equilibration. Runs of 0.8 ns were initially performed to equilibrate the systems. Then, the simulations were run for additional 1 ns for data collection. The trigger values and details of local equilibration involved in the RMD algorithm are the same as that employed in bulk water.

Three systems were examined with the above simulation parameters. Simulations of pure confined water (500 molecules) were conducted to benchmark the diffusivities of the TIP3P water model under confinement. A reactive and non-reactive system consisting of water and hydronium are the other two systems considered. A reactive system allows for the structural diffusion and was used to analyse the transport properties of the charge. Non-reactive systems in which the RMD algorithm was not implemented (absence of structural diffusion) were studied to compare the diffusion of the hydronium ion with the vehicular component of the charge in the reactive system.

CNTs of lower radius such as 4.07 Å ($R = 6$), where water wires may theoretically exist, were not studied. The parameterisation of this RMD algorithm is based on the complex 3D hydrogen-bonding network. It is an interesting possibility whether relaxations of the solvation triggers will allow the RMD algorithm to be applied to more confined systems, but that avenue is not pursued in this work, where we strictly adhere to the bulk water RMD parameters.

3. Results and discussion

The effect of confinement within CNTs on some of the physical and transport properties of the proton and water is illustrated here in detail as a function of CNT radius. The snapshots of a portion of the water and hydronium ion confined in the five CNTs are shown in Figure 2. It is immediately apparent from these snapshots that the hydronium ion is preferentially located at the water–CNT interface with the oxygen atom extended towards the CNT. Both of these visual observations from the snapshots will be discussed in a more quantitative nature below.

3.1 Radial density profile

The distribution profiles of water molecules in confined geometries have been widely studied [56–58]. Figure 3(a) represents the density profile of water in a non-reactive system along the radial distance for different channel radii. The density near the CNT wall decreases with the channel radius. The number of peaks in the radial density profile increases as the CNT radius increases, implying the increase in water layers within the tube. At larger CNT radii, the density near the centre of the tube approaches the

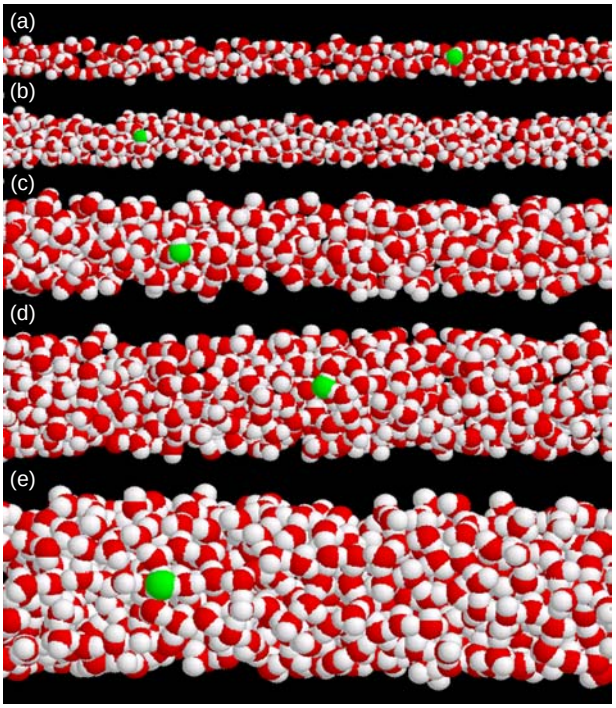

Figure 2. Snapshot of a portion of the CNTs studied whose radii are (a) 5.42 Å, (b) 6.78 Å, (c) 8.14 Å, (d) 9.49 Å and (e) 10.85 Å. O of H_3O^+, green; O of H_2O, red; H, white.

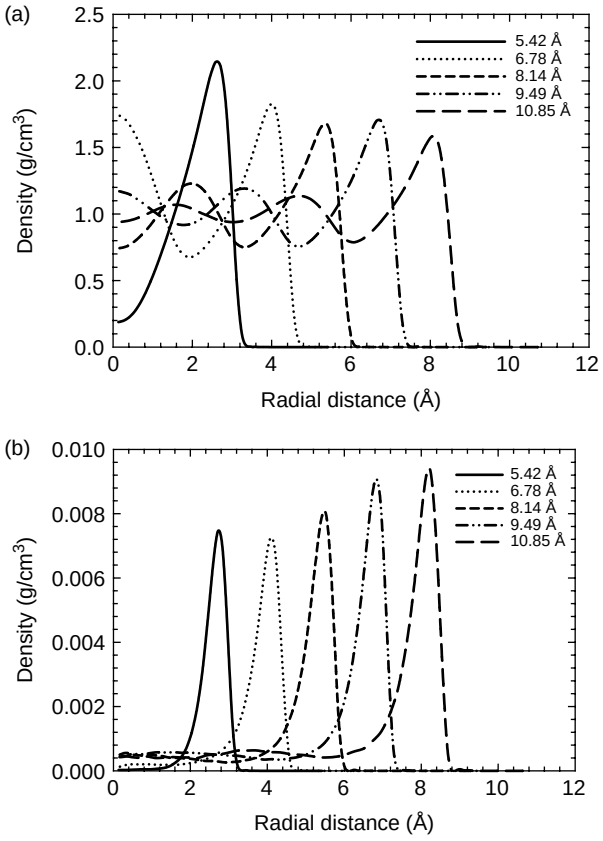

Figure 3. Radial density profile of (a) water and (b) hydronium confined in CNTs with different radii in the non-reactive system.

bulk water density, which indicates that as the channel radius increases we find bulk water behaviour towards the centre of the tube where the fluid–tube interaction is weak. In other works, where the CNTs are modelled atomistically both ordered structures (helical [59] or *n*-gonal rings [60], where *n* is based on the radius) and organised layers were observed depending on the geometry of the CNT, pressure, temperature, water model and many other simulation parameters.

Figure 3(b) shows the radial density profile of the hydronium ion in a non-reactive system for different CNT radii. Unlike water, the density near the wall increases as the channel radius increases. From both figures, we can observe that the position of the first peak of the hydronium ion is always closer to the wall than the first peak of water. The very high first peak also shows that the hydronium ion is preferentially located next to the walls. The probability distribution of the orientation of the hydronium ion in the outer and inner layers of the CNT of radius 10.85 Å in the non-reactive system is presented in Figure 4. The outer layer is defined 2 Å from the accessible radius. The orientation of the hydronium axis (originating at the midpoint of the three hydrogen atoms and terminating at the position of oxygen atom) is measured with respect to the radial axis. An angle of 0° corresponds to the oxygen atom pointing towards the tube wall. The distribution of orientation in the outer layer shows a strong preference for the ion to be oriented with the oxygen atom, protruding towards the wall with the hydrogen atoms forming hydrogen bonds with the water molecules in the CNT. However, at the inner layers, no such strong preference for a particular orientation is observed. Similar affinity for the interface and preferential orientation of the hydronium ion has been observed at the interface between a liquid and hydrophobic media or vapour both from simulation [61–64] and experiments [65–67]. The reason behind this phenomenon has been attributed to the energetically favourable formation of hydrogen bonds by the hydronium ion with three water molecules without strongly perturbing the hydrogen-bonding network in the aqueous phase.

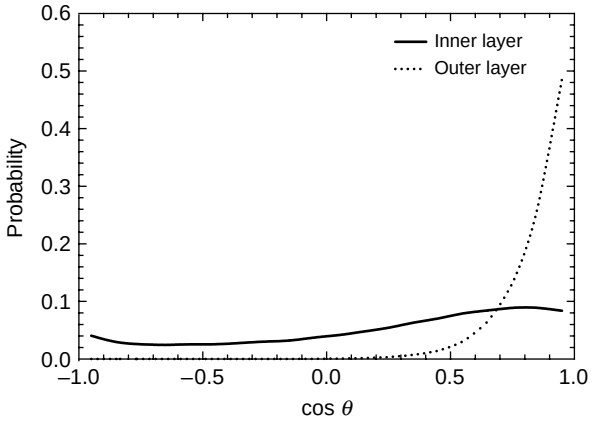

Figure 4. Probability distribution of the orientation of the hydronium ion with respect to the radial axis in the outer (dotted line) and inner layers (solid line) of the CNT with radius 10.85 Å. Measurement of $\cos\theta = 1$ corresponds to the oxygen atom pointing towards the wall.

3.2 *Reaction rate constant*

The hopping of the proton can be quantitatively described either in terms of lifetime of the proton or hopping rate. Here, we denote it by reaction rate constant since the structural diffusion is considered as a reaction. The rate constant, *k*, is calculated using the expression:

$$k = \frac{N_{\text{react}}}{\text{time}\cdot V_{\text{tube}}} \times \frac{1}{[H_2O][H_3O^+]}, \tag{4}$$

where V_{tube} is the accessible nanotube volume excluding the void space near the wall, N_{react} is the number of reactions taken place, 'time' is the length of the simulation and the square brackets represent the concentration. The concentrations and V_{tube} are the same for all the CNTs considered, since they all have the same density. The definition of reaction needs to be clearly explained in this aspect. The rattling of proton between the reactants is observed in our simulation but they are not taken into account for the calculation of rate constant. At the end of rattling, the proton might end up either in the parent water molecule (starting molecule of rattle) or a different water molecule. In either case, we consider a reaction has occurred at the end of rattling. The above definition of reaction is chosen to be consistent with the definition of reaction for proton transport in bulk water [14] whose trigger values are being used. Analysis of the reaction rates of different CNTs shown in Figure 5 indicates that there is an upward trend with the tube radius. The reaction rate has increased by roughly an order of magnitude from the smallest to the largest tube. For comparison, the reaction

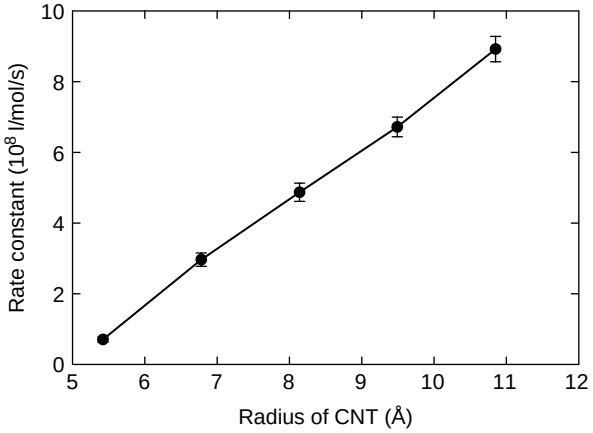

Figure 5. Reaction rate constant, *k*, as a function of CNT radius. An increase in *k* is observed with the increase in the radius.

rate constant for structural diffusion of proton in bulk water from the experiment [68] is 1.072×10^{10} l/mol/s. The reaction rate constant for structural diffusion of proton in bulk water from the RMD algorithm is 1.090×10^{10} l/mol/s [14]. Both bulk reaction rates are about an order of magnitude higher than the rate constants found even in the largest CNT studied here.

The reduction in the rate constant can be directly related to the decrease in the probability of the occurrence of reaction. In the RMD algorithm, the event of the reaction is based on the satisfaction of triggers. The fraction satisfying each trigger is presented in Figure 6. The order of the trigger analysed in the plot is based on the hierarchy on which it was verified during the simulation. The particular hierarchy was chosen for computational efficiency and the satisfaction of a particular trigger was tested only when the previous trigger was satisfied. Figure 6 contains only six triggers listed, since each fraction was calculated based on the satisfaction of the earlier trigger. Therefore, the first trigger, $r_{\mathrm{OO,Zundel}}$, provided the basis for the calculation of the fraction satisfying the second trigger. Though the preferential location and orientation of the hydronium ions at the wall affect the satisfaction of the geometric trigger, the energetic trigger is identified as the one most affected by confinement and causes a reduction in the structural diffusivity.

Another interesting way to analyse the effect of confinement on the reaction rate constant is to study the reactivity profile along the radial distance. For this purpose, we have chosen the CNT with radius 10.85 Å where the maximum number of reactions takes place. The CNT is divided into cylindrical shells and the number of reactions in each shell is based on the position of the reacting hydronium. The rattling of protons is included in the rate calculation. The reaction rate is provided in Figure 7 as a function of the radial distance along with the hydronium concentration. The hydronium ion concentration near the wall is nearly 10 times higher than that in the inner layers of the CNT. Typically, one considers a reaction rate constant, as shown in Equation (4), to be independent of concentration. If this was the case, then we would expect the rate to increase by nearly a factor of 10 near the wall. Since we do not see this, we can conclude that the reaction rate constant is not independent of the local concentration and, in fact, decreases with increasing hydronium concentration. This same decrease in rate constant with increasing hydronium ion concentration is also observed in the aqueous HCl system [14], although to a lesser extent.

3.3 *Water diffusivity*

The diffusion coefficient of bulk water can be calculated using the Einstein expression, which relates the diffusivity to the mean square displacement (MSD) of a molecule as

$$D = \lim_{\tau \to \infty} \frac{\langle [r(t+\tau) - r(t)]^2 \rangle}{2d\tau}, \tag{5}$$

where d is the dimensionality of the system and τ is the observation time. In the CNT, we apply this expression to evaluate the diffusion coefficient in only the axial dimension.

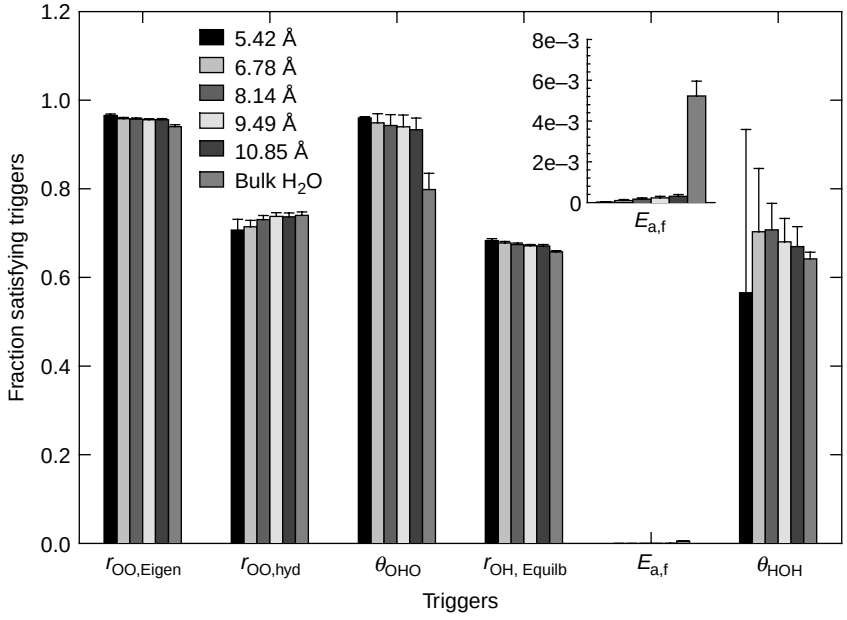

Figure 6. Histogram of the fraction satisfying the geometric and energetic triggers in the various CNTs studied. Each fraction is calculated based on the satisfaction of the previous trigger. Data from bulk water are also included to observe the effect of confinement on trigger satisfaction.

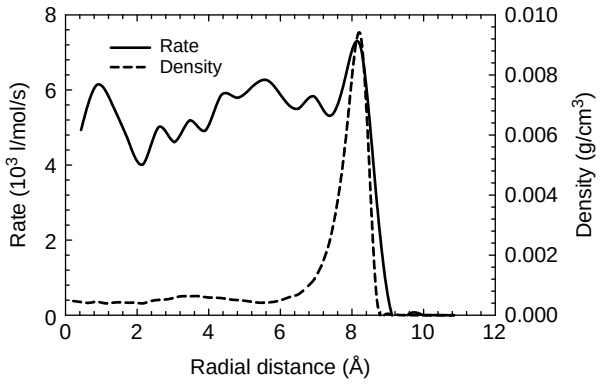

Figure 7. Rate, r, profile (solid line) along the radial distance of CNT of radius 10.85 Å. The radial hydronium concentration profile (dashed line) is provided to analyse the effect of the concentration on rate under confinement.

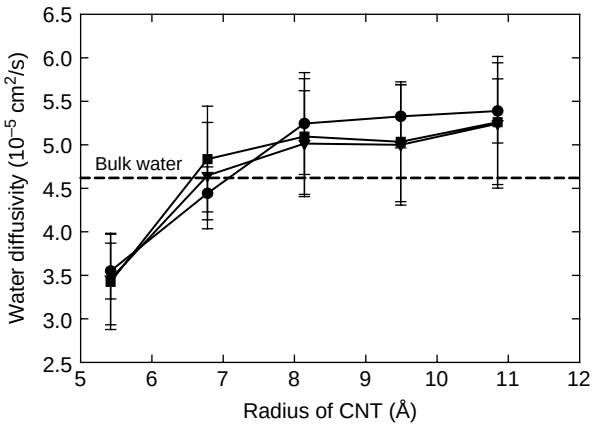

Figure 8. Water diffusivity along the tube axis for the (i) pure confined water system, solid circles, (ii) non-reactive system, solid triangles, (iii) reactive system, solid squares expressed as a function of CNT radius. The dashed line represents the bulk water diffusivity of a TIP3P model at 300 K.

Since the movement of the molecules is restricted by confinement in the other two directions (radial axis), the trajectories would not reach the long-time limit required by the Einstein relation in the radial dimension. In a confined geometry, the diffusion of water can be described by three mechanisms: [69] Fickian (MSD $\propto \tau$), single file (MSD $\propto \tau^{1/2}$) and ballistic (MSD $\propto \tau^2$). Single file motion will be observed only if the pore is so small that water molecules cannot pass each other within the tube [70]. This is not the case in any of these simulations. Striolo [69] observed the molecules in the CNT (8,8) to initially follow a ballistic transport but in the long run evolve into Fickian diffusion. Therefore, in the CNTs considered, we expect the Fickian diffusion in the long-time limit.

We have calculated the water diffusivity in the axial direction in all the three systems considered. Axial diffusivity measurement in pure confined water and non-reactive systems can be done without ambiguity, while the reactive system which involves the change in the identity of the molecules needs attention. Therefore, instead of calculating the diffusivity through the entire simulation time involving reactions, we calculated the water diffusivities in the reactive system for time segments in which they did not react. Figure 8 shows the axial water diffusivity in the various systems against CNT radius along with the bulk water density at 300 K. The reason we compare the diffusivities of three systems is to show that the presence of the hydronium ion and the implementation of the RMD algorithm do not affect the water diffusivity. The diffusivities of all the three systems are almost the same. They initially increase with the channel radius but later stabilise. At larger radii, we find the water diffusivity to be slightly higher than the bulk water diffusivity. This might be explained due to the fact that the choice of accessible volume impacts the fluid density, which can have considerable influence on the diffusion coefficient. For example, when the CNT of radius 10.85 Å has its density changed from 0.9965 to 1.15 g/cm^3, it causes a 22% reduction in the water diffusivity.

Liu et al. [59] measured the diffusivity of water in an atomistically modelled armchair (R,R) CNT with indices $R = 8$, 10, 12, 14, 16 and found a steady increase in the water axial diffusivity with the increase in radius and found values below that of their bulk water diffusivity. With the increase in confinement of channels (from 5 to 2 Å), Brewer et al. [36] observed a similar trend of decrease in the water diffusivity, which was also less than the bulk phase.

3.4 Charge diffusivity

The transport properties of the charge and its components were measured using the Einstein relation. In the non-reactive system, the diffusivity of the charge is equal to the vehicular diffusion of the hydronium ion. In the RMD simulation, the excess charge hops from one water molecule to another, temporarily creating hydronium ions from each molecule. The hydronium ion trajectories can be unambiguously followed using the centre-of-mass position of the ion. Decoupling the total charge movement into the two components can be easily done by enforcing the following relationship:

$$\Delta\vec{r}_{\text{tot}} = \Delta\vec{r}_{\text{veh}} + \Delta\vec{r}_{\text{struct}}. \tag{6}$$

By the implementation of the above constraint in each step, the total displacement vector is equal to the sum of the displacement vectors attributed by both the vehicular and structural components. Similar decomposition of the total charge displacement vector has been performed earlier [71]. The vehicular component is continuously measured whether a reaction takes place or not. During the absence of reaction, the displacement due to structural

diffusion is zero and the vehicular component is the sole contributor to the total charge diffusion. When a reaction takes place, the displacement due to the Newtonian motion (MD step) is categorised as the vehicular contribution, while the displacement of the reactant hydronium from the location before reaction (position at the end of MD step) to the final position of the product hydronium after local equilibration is considered as the structural displacement. The relationship between the vehicular, D_{veh}, structural, D_{struct}, and total charge diffusion, D_{tot}, can be obtained by substituting Equation (6) in Einstein's relation (Equation (5)) as follows:

$$D_{\text{tot}} = \lim_{\tau\to\infty} \frac{\left\langle \Delta\vec{r}^{\,2}_{\text{veh}} \right\rangle + \left\langle \Delta\vec{r}^{\,2}_{\text{struct}} \right\rangle + 2\langle \Delta\vec{r}_{\text{veh}} \Delta\vec{r}_{\text{struct}} \rangle}{2d\tau}. \quad (7)$$

By making an arbitrary but reasonable definition of decomposition, we get:

$$D_{\text{veh}} \equiv \lim_{\tau\to\infty} \frac{\left\langle \Delta\vec{r}^{\,2}_{\text{veh}} \right\rangle}{2d\tau}, \quad (7a)$$

$$D_{\text{struct}} \equiv \lim_{\tau\to\infty} \frac{\langle \Delta\vec{r}^{\,2}_{\text{struct}} \rangle}{2d\tau}, \quad (7b)$$

$$D_{\text{corr}} \equiv \lim_{\tau\to\infty} \frac{2\langle \Delta\vec{r}_{\text{veh}} \Delta\vec{r}_{\text{struct}} \rangle}{2d\tau}, \quad (7c)$$

where D_{corr} is the correlation term that denotes the coupling between the structural and vehicular contributions. If $D_{\text{corr}} = 0$, then both the components of the total charge diffusion are uncorrelated. Analogous to the estimation of water diffusion coefficients, we have reported only the diffusivities of the charge in the axial direction.

The total charge diffusivity and the individual contributions of the two diffusion mechanisms in the axial direction for the various CNTs considered are shown in Figure 9, along with the vehicular diffusion of hydronium in the non-reactive system. The uncertainties are represented as the standard error [72]. The total diffusion and vehicular component follow the same trend where an initial increase in the radius of CNT caused a steep increase in the axial diffusivities and further reduction in the confinement (radius $>$ 8.14 Å) did not affect them tremendously. On the other hand, the structural component showed a steady increase with the reduction of confinement.

The implementation of the RMD algorithm should not affect the fluid vehicular diffusivities. Similar to the case of measurement of water diffusivity, the vehicular diffusion of the hydronium ion in a non-reactive system is compared to the vehicular component of charge diffusion in a reactive system and is found to be in agreement within the standard errors.

A better way to understand the effect of confinement on the charge diffusion would be to compare these

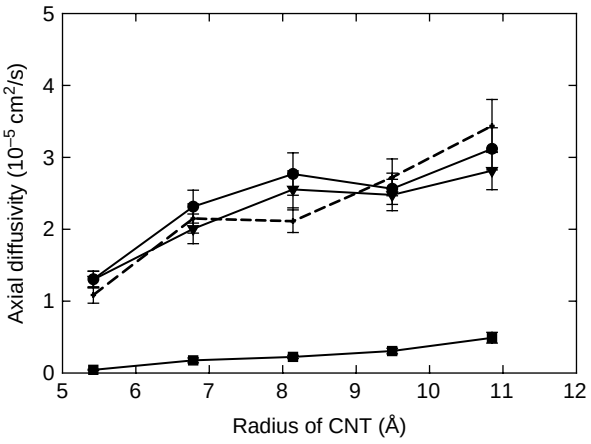

Figure 9. The axial total charge diffusivity (solid circles) and its two components (i) vehicular (solid triangles) and (ii) structural component (solid squares) for the various CNTs studied in a reactive system. The dashed line represents the vehicular diffusion of H_3O^+ in the non-reactive system.

diffusivity values to that of bulk water from our previous work. The total, structural and vehicular diffusivities of proton in bulk water at 300 K are 7.33×10^{-5}, 4.29×10^{-5} and 2.83×10^{-5} cm^2/s based on our algorithm [14]. When we compare these values to the CNT with the largest radius, we find that the vehicular diffusivities are virtually the same while the structural component is only 12% of the value observed in bulk water. This can be explained by the obvious reduction in the rate constant. So, in overall, there is 58% reduction in the total charge diffusion at our largest CNT due to confinement.

We found the two components of charge diffusivity in bulk water to be uncorrelated and structural diffusion contributing to about 60% of the charge diffusion. The vehicular component is the major contributor of the charge diffusion in CNTs for the range of radius we investigated, and both the components are uncorrelated. We can also conclude that the confinement affects the structural diffusion much more than the vehicular diffusion.

Proton transport in confined water has been previously studied. The mobility of proton was much higher [34,37] in 1D water wires in armchair (6,6) CNTs (radius = 4.07 Å) than observed in bulk water. However, in cylindrical channels with 3D water structure, the proton diffusivity was computed to be much lower than that observed in bulk water but increased with channel diameter [36]. The centre of excess charge diffusion coefficient in a cylindrical channel of carbon with radius and length of 5 and 29.8 Å, respectively, containing 77 water molecules was about 2.5×10^{-5} cm^2/s [36] compared to the computed value of $4.5 \pm 1.1 \times 10^{-5}$ cm^2/s in bulk water using the MS-EVB model. The charge diffusivity at our smallest CNT of radius 5.42 Å is 1.30×10^{-5} cm^2/s compared to the value of 7.33×10^{-5} cm^2/s in bulk water. Therefore, we observe

the same qualitative trend with the RMD algorithm as is observed with the MS-EVB model.

4. Conclusions

Proton mobility through water confined in CNTs of radii ranging from 5.42 to 10.85 Å at 300 K and infinite dilution has been investigated by means of classical MD simulations with the structural diffusion modelled with an RMD algorithm. The algorithm, parameterised for a bulk water system, was directly implemented to the CNT systems without any modifications. The algorithm has successfully captured the essential features of the structural diffusion under confinement, confirming its facile adaptability to different environments.

The radial density profiles of both water and hydronium ions were computed. The radial water profile showed layered structures in the confined geometries with higher density near the walls and an increase in the number of layers with increasing radius. Hydronium ions showed a great affinity towards the wall and were preferentially oriented with the oxygen atom facing the wall. The reaction rate constant for the proton transfer process increased with the decrease in confinement due to requirement imposed by the energetic trigger. The axial water diffusivity was not affected by the presence of protons in dilute concentrations or by the implementation of the RMD algorithm. The diffusion coefficients initially increased with the increase in the radius of the CNT but approached a plateau at the larger tube sizes. The axial vehicular diffusion of hydronium ions showed analogous behaviour. The axial structural component of charge diffusion showed a steady increase with increasing diameter of the CNT. The two components were determined to be uncorrelated with the axial total charge diffusivity, essentially being the sum of the two components. We observed that the vehicular component of the charge diffusivity was the same as that in bulk water in the largest diameter CNT. However, the structural component of charge diffusivity was only 12% of the value observed in bulk water. Clearly, confinement impacts structural diffusion at larger tube sizes and in a more significant manner than vehicular diffusion.

This work impacts the design of novel PEMs because it indicates that a severe reduction in the structural component of the charge diffusivity occurs as a consequence of confinement. The coupled effects of confinement and high acidity, as present in PEMs, remain of interest.

Acknowledgements

This work is funded by the US Department of Energy (DOE) BES under contract number DE-FG02-05ER15723. This research used resources of the Center for Computational Sciences at Oak Ridge National Laboratory (ORNL) supported by the Office of Science of the DOE (contract number DE-AC05-00OR22725) and National Institute for Computational Sciences (NICS) supported by the National Science Foundation (agreement number OCI 07-11134).

References

[1] K.D. Kreuer, *On the development of proton conducting polymer membranes for hydrogen and methanol fuel cells*, J. Membr. Sci. 185 (2001), pp. 29–39.
[2] K.D. Kreuer, M. Schuster, B. Obliers, O. Diat, U. Traub, A. Fuchs, U. Klock, S.J. Paddison, and J. Maier, *Short-side-chain proton conducting perfluorosulfonic acid ionomers: Why they perform better in PEM fuel cells*, J. Power Sources 178 (2008), pp. 499–509.
[3] N. Agmon, *The Grotthuss mechanism*, Chem. Phys. Lett. 244 (1995), pp. 456–462.
[4] M. Tuckerman, K. Laasonen, M. Sprik, and M. Parrinello, Ab inito *molecular dynamics simulation of the solvation and transport of hydronium and hydroxyl ions in water*, J. Chem. Phys. 103 (1995), pp. 150–161.
[5] D. Marx, M.E. Tuckerman, J. Hutter, and M. Parrinello, *The nature of the hydrated excess proton in water*, Nature 397 (1999), pp. 601–604.
[6] R.A. Robison and R.H. Stokes, *Electrolyte Solutions*, Butterworths, London, 1959.
[7] G. Zundel and H. Metzger, *Energy bands of excess tunneling protons in fluid acids. IR spectroscopy of $H_5O_2^+$ groups*, Z. Phys. Chem. 58 (1968), pp. 225–245.
[8] E. Wicke, M. Eigen, and T. Ackermann, *Über den zustand des protons (hydronium-ions) in wäbriger lösung*, Z. Phys. Chem. 1 (1954), pp. 340–364.
[9] O. Markovitch, H. Chen, S. Izvekov, F. Paesani, G.A. Voth, and N. Agmon, *Special pair dance and partner selection: Elementary steps in proton transport in liquid water*, J. Phys. Chem. B 112 (2008), pp. 9456–9466.
[10] S.J. Paddison, G. Bender, K.D. Kreuer, N. Nicoloso, and T.A. Zawodzinski, *The microwave region of the dielectric spectrum of hydrated Nafion® and other sulfonated membranes*, J. New Mater. Electrochem. Syst. 3 (2000), pp. 291–300.
[11] Z.J. Lu, M. Lanagan, E. Manias, and D.D. Macdonald, *Two-port transmission line technique for dielectric property characterization of polymer electrolyte membranes*, J. Phys. Chem. B 113 (2009), pp. 13551–13559.
[12] R. Paul and S.J. Paddison, *A statistical mechanical model for the calculation of the permittivity of water in hydrated polymer electrolyte membrane pores*, J. Chem. Phys. 115 (2001), pp. 7762–7771.
[13] R. Paul and S.J. Paddison, *Structure and dielectric saturation of water in hydrated polymer electrolyte membranes: Inclusion of the internal field energy*, J. Phys. Chem. B 108 (2004), pp. 13231–13241.
[14] M. Esai Selvan, D.J. Keffer, S. Cui, and S.J. Paddison, *A reactive molecular dynamics algorithm for proton transport in aqueous systems*, J. Chem. Phys. C, under review.
[15] T.A. Zawodzinski, T.E. Springer, J. Davey, R. Jestel, C. Lopez, J. Valerio, and S. Gottesfeld, *A comparative-study of water-uptake by and transport through ionomeric fuel-cell membranes*, J. Electrochem. Soc. 140 (1993), pp. 1981–1985.
[16] K.D. Kreuer, *On the development of proton conducting materials for technological applications*, Solid State Ion 97 (1997), pp. 1–15.
[17] S.J. Paddison and R. Paul, *The nature of proton transport in fully hydrated Nafion®*, Phys. Chem. Chem. Phys. 4 (2002), pp. 1158–1163.
[18] K.D. Kreuer, S.J. Paddison, E. Spohr, and M. Schuster, *Transport in proton conductors for fuel-cell applications: Simulations, elementary reactions, and phenomenology*, Chem. Rev. 104 (2004), pp. 4637–4678.
[19] M.K. Petersen, F. Wang, N.P. Blake, H. Metiu, and G.A. Voth, *Excess proton solvation and delocalization in a hydrophilic pocket of the proton conducting polymer membrane nafion*, J. Phys. Chem. B 109 (2005), pp. 3727–3730.
[20] K.D. Kreuer, *On the complexity of proton conduction phenomena*, Solid State Ion. 136 (2000), pp. 149–160.
[21] S.J. Paddison, *Proton conduction mechanisms at low degrees of hydration in sulfonic acid-based polymer electrolyte membranes*, Ann. Rev. Mater. Res. 33 (2003), pp. 289–319.

[22] M. Eikerling, S.J. Paddison, L.R. Pratt, and T.A.J. Zawodzinski, *Defect structure for proton transport in a triflic acid monohydrate solid*, Chem. Phys. Lett. 368 (2003), pp. 108–114.

[23] R.L. Hayes, S.J. Paddison, and M.E. Tuckerman, *Proton transport in triflic acid hydrates studied via path integral Car–Parrinello molecular dynamics*, J. Chem. Phys. B 113 (2009), pp. 16574–16589.

[24] R. Car and M. Parrinello, *Unified approach for molecular-dynamics and density-functional theory*, Phys. Rev. Lett. 55 (1985), pp. 2471–2474.

[25] S.R. Billeter and W.F. van Gunsteren, *Protonizable water model for quantum dynamical simulations*, J. Phys. Chem. A 102 (1998), pp. 4669–4678.

[26] P. Intharathep, A. Tongraar, and K. Sagarik, Ab initio *QM/MM dynamics of* H_3O *in water*, J. Comput. Chem. 27 (2006), pp. 1723–1732.

[27] A. Warshel and R.M. Weiss, *An empirical valence bond approach for comparing reactions in solutions and in enzymes*, J. Am. Chem. Soc. 102 (1980), pp. 6218–6226.

[28] U.W. Schmitt and G.A. Voth, *The computer simulation of proton transport in water*, J. Chem. Phys. 111 (1999), pp. 9361–9381.

[29] F. Wang and G.A. Voth, *A linear-scaling self-consistent generalization of the multistate empirical valence bond method for multiple excess protons in aqueous systems*, J. Chem. Phys. 122 (2005), pp. 144105-1–9.

[30] Y.J. Wu, H.N. Chen, F. Wang, F. Paesani, and G.A. Voth, *An improved multistate empirical valence bond model for aqueous proton solvation and transport*, J. Phys. Chem. B 112 (2008), pp. 467–482.

[31] R.G. Schmidt and J. Brickmann, *Molecular dynamics simulation of the proton transport in water*, Ber. Bunsen-Ges. Phys. Chem. Chem. Phys. 101 (1997), pp. 1816–1827.

[32] M.A. Lill and V. Helms, *Molecular dynamics simulation of proton transport with quantum mechanically derived proton hopping rates (Q-HOP MD)*, J. Chem. Phys. 115 (2001), pp. 7993–8005.

[33] B.W. Jiang, M.E. Selvan, D.J. Keffer, and B.J. Edwards, *A reactive molecular dynamics study of the thermal decomposition of perfluorodimethyl ether*, J. Phys. Chem. B 113 (2009), pp. 13670–13677.

[34] D.J. Mann and M.D. Halls, *Water alignment and proton conduction inside carbon nanotubes*, Phys. Rev. Lett. 90 (2003), pp. 195503-1–4.

[35] S.H. Lee, H^+ *ion migration in water filled carbon nanotube*, Bull. Korean Chem. Soc. 30 (2009), pp. 700–702.

[36] M.L. Brewer, U.W. Schmitt, and G.A. Voth, *The formation and dynamics of proton wires in channel environments*, Biophys. J. 80 (2001), pp. 1691–1702.

[37] C. Dellago, M.M. Naor, and G. Hummer, *Proton transport through water-filled carbon nanotubes*, Phys. Rev. Lett. 90 (2003), pp. 105902-1–4.

[38] J.K. Holt, *Carbon nanotubes and nanofluidic transport*, Adv. Mater. 21 (2009), pp. 3542–3550.

[39] A. Alexiadis and S. Kassinos, *The density of water in carbon nanotubes*, Chem. Eng. Sci. 63 (2008), pp. 2047–2056.

[40] G. Hummer, J.C. Rasaiah, and J.P. Noworyta, *Water conduction through the hydrophobic channel of a carbon nanotube*, Nature 414 (2001), pp. 188–190.

[41] R.M. LyndenBell and J.C. Rasaiah, *Mobility and solvation of ions in channels*, J. Chem. Phys. 105 (1996), pp. 9266–9280.

[42] M.C. Gordillo and J. Marti, *Hydrogen bond structure of liquid water confined in nanotubes*, Chem. Phys. Lett. 329 (2000), pp. 341–345.

[43] B.K. Peterson, J. Walton, and K.E. Gubbins, *Fluid behavior in narrow pores*, J. Chem. Soc., Faraday Trans. 82 (1986), pp. 1789–1800.

[44] C.L. McCallum, T.J. Bandosz, S.C. McGrother, E.A. Muller, and K.E. Gubbins, *A molecular model for adsorption of water on activated carbon: Comparison of simulation and experiment*, Langmuir 15 (1999), pp. 533–544.

[45] W.A. Steele, *The Interaction of Gases with Solid Surfaces*, Pergamon Press, Oxford, 1974.

[46] G.S. Kell, *Density, thermal expansivity, and compressibility of liquid water from 0 to 150°C – Correlations and tables for atmospheric-pressure and saturation reviewed and expressed on 1968 temperature scale*, J. Chem. Eng. Data 20 (1975), pp. 97–105.

[47] S.T. Cui, J.W. Liu, M. Esai Selvan, D.J. Keffer, B.J. Edwards, and W.V. Steele, *A molecular dynamics study of a nafion polyelectrolyte membrane and the aqueous phase structure for proton transport*, J. Phys. Chem. B 111 (2007), pp. 2208–2218.

[48] W.L. Jorgensen, J.J. Chandrasekhar, J.D. Madura, R.W. Impey, and M.L. Klein, *Comparison of simple potential functions for simulating liquid water*, J. Chem. Phys. 79 (1983), pp. 926–935.

[49] E. Neria, S. Fischer, and M. Karplus, *Simulation of activation free energies in molecular systems*, J. Chem. Phys. 105 (1996), pp. 1902–1921.

[50] S. Urata, J. Irisawa, A. Takada, W. Shinoda, S. Tsuzuki, and M. Mikami, *Molecular dynamics simulation of swollen membrane of perfluorinated ionomer*, J. Phys. Chem. B 109 (2005), pp. 4269–4278.

[51] G. Hummer, D.M. Soumpasis, and M. Neumann, *Pair correlations in an NaCl-SPC water model – Simulations vs. extended RISM computations*, Mol. Phys. 77 (1992), pp. 769–785.

[52] M. Tuckerman, B.J. Berne, and G.J. Martyna, *Reversible multiple time scale molecular-dynamics*, J. Chem. Phys. 97 (1992), pp. 1990–2001.

[53] S. Nosé, *A unified formulation of the constant temperature molecular-dynamics methods*, J. Chem. Phys. 81 (1984), pp. 511–519.

[54] S. Nosé, *A molecular dynamics method for simulations in the canonical ensemble*, Mol. Phys. 52 (1984), pp. 255–268.

[55] W.G. Hoover, *Canonical dynamics: Equilibrium phase-space distributions*, Phys. Rev. A 31 (1985), pp. 1695–1697.

[56] P. Gallo, M.A. Ricci, and M. Rovere, *Layer analysis of the structure of water confined in vycor glass*, J. Chem. Phys. 116 (2002), pp. 342–346.

[57] P. Hirunsit and P.B. Balbuena, *Effects of confinement on water structure and dynamics: A molecular simulation study*, J. Phys. Chem. C 111 (2007), pp. 1709–1715.

[58] G. Cicero, J.C. Grossman, E. Schwegler, F. Gygi, and G. Galli, *Water confined in nanotubes and between graphene sheets: A first principle study*, J. Am. Chem. Soc. 130 (2008), pp. 1871–1878.

[59] Y.C. Liu, Q. Wang, T. Wu, and L. Zhang, *Fluid structure and transport properties of water inside carbon nanotubes*, J. Chem. Phys. 123 (2005), pp. 234701-1–7.

[60] R.J. Mashl, S. Joseph, N. Aluru, and E. Jakobsson, *Effects of hydrophobic channels on water structure and dynamics*, Biophys. J. 84 (2003), pp. 488A–489A.

[61] R. Vacha, D. Horinek, M.L. Berkowitz, and P. Jungwirth, *Hydronium and hydroxide at the interface between water and hydrophobic media*, Phys. Chem. Chem. Phys. 10 (2008), pp. 4975–4980.

[62] M.K. Petersen, S.S. Iyengar, T.J.F. Day, and G.A. Voth, *The hydrated proton at the water liquid/vapor interface*, J. Phys. Chem. B 108 (2004), pp. 14804–14806.

[63] M. Esai Selvan, J. Liu, D.J. Keffer, S. Cui, B.J. Edwards, and W.V. Steele, *Molecular dynamics study of structure and transport of water and hydronium ions at the membrane/vapor interface of nafion*, J. Phys. Chem. C 112 (2008), pp. 1975–1984.

[64] H.S. Lee and M.E. Tuckerman, Ab initio *molecular dynamics studies of the liquid–vapor interface of an HCl solution*, J. Phys. Chem. A 113 (2009), pp. 2144–2151.

[65] P.B. Miranda and Y.R. Shen, *Liquid interfaces: A study by sum-frequency vibrational spectroscopy*, J. Phys. Chem. B 103 (1999), pp. 3292–3307.

[66] S. Gopalakrishnan, D.F. Liu, H.C. Allen, M. Kuo, and M.J. Shultz, *Vibrational spectroscopic studies of aqueous interfaces: Salts, acids, bases, and nanodrops*, Chem. Rev. 106 (2006), pp. 1155–1175.

[67] C.S. Tian, N. Ji, G.A. Waychunas, and Y.R. Shen, *Interfacial structures of acidic and basic aqueous solutions*, J. Am. Chem. Soc. 130 (2008), pp. 13033–13039.

[68] Z. Luz and S. Meiboom, *Activation energies of proton transfer reactions in water*, J. Am. Chem. Soc. 86 (1964), pp. 4768–4769.

[69] A. Striolo, *The mechanism of water diffusion in narrow carbon nanotubes*, Nano. Lett. 6 (2006), pp. 633–639.

[70] D. Keffer, A.V. McCormick, and H.T. Davis, *Unidirectional and single-file diffusion in alpo4-5: Molecular dynamics investigations*, Mol. Phys. 87 (1996), pp. 367–387.

[71] M.K. Petersen and G.A. Voth, *Characterization of the solvation and transport of the hydrated proton in the perfluorosulfonic acid membrane nafion*, J. Phys. Chem. B 110 (2006), pp. 18594–18600.

[72] H. Flyvbjerg and H.G. Petersen, *Error-estimates on averages of correlated data*, J. Chem. Phys. 91 (1989), pp. 461–466.